Anomalous Diffusion of Proteins Due to Molecular Crowding

Daniel S. Banks* and Cécile Fradin*†
*Department of Physics and Astronomy, and †Department of Biochemistry and Biomedical Sciences, McMaster University, Hamilton, Ontario, Canada

ABSTRACT We have studied the diffusion of tracer proteins in highly concentrated random-coil polymer and globular protein solutions imitating the crowded conditions encountered in cellular environments. Using fluorescence correlation spectroscopy, we measured the anomalous diffusion exponent α characterizing the dependence of the mean-square displacement of the tracer proteins on time, $\langle r^2(t)\rangle \sim t^{\alpha}$. We observed that the diffusion of proteins in dextran solutions with concentrations up to 400 g/l is subdiffusive ($\alpha < 1$) even at low obstacle concentration. The anomalous diffusion exponent α decreases continuously with increasing obstacle concentration and molecular weight, but does not depend on buffer ionic strength, and neither does it depend strongly on solution temperature. At very high random-coil polymer concentrations, α reaches a limit value of $\alpha_l \approx 3/4$, which we take to be the signature of a coupling between the motions of the tracer proteins and the segments of the dextran chains. A similar, although less pronounced, subdiffusive behavior is observed for the diffusion of streptavidin in concentrated globular protein solutions. These observations indicate that protein diffusion in the cell cytoplasm and nucleus should be anomalous as well, with consequences for measurements of solute diffusion coefficients in cells and for the modeling of cellular processes relying on diffusion.

INTRODUCTION

A detailed understanding of the diffusion of proteins in solutions containing high concentrations of soluble macromolecules is presently lacking. However, such an understanding is needed to correctly model passive intracellular transport, a process likely to regulate important cellular functions such as signal transduction (1,2), self-assembly of supramolecular structures (3), gene transcription (4), kinetics of reaction (5), embryogenesis (6), or regulation of cell polarization (7). This understanding would also be beneficial to several important fields of studies across disciplines. In the fields of physical chemistry of solutions and polymer physics, it would facilitate the resolution of long-standing fundamental questions such as the clarification of the mechanisms that govern the dynamics of single chains in polymer solutions and the determination of the relationship between the macroscopic and microscopic viscosities of these solutions (8–10). In pharmaceutical research, it would permit the improvement of drug delivery systems relying on the slow release of drugs from polymer matrices (11,12).

Molecular crowding affects solute diffusion by increasing the effective viscosity of the medium (13). It is also known to cause depletion interactions, which tend to segregate macromolecules according to their size due to the increase in free volume accessible to the solutes upon segregation (14) and to affect the rates of chemical reactions taking place in solution (13,15). In cells, for example, it is thought to influence not only protein and nucleic acid diffusion, but also molecular recognition (16), protein assembly (17), and protein folding (9,18). However, despite its crucial importance, diffusion in crowded environments remains a challenge to study and predict. Even in simple model systems such as concentrated polymer solutions none of the many models proposed can fully describe the body of experimental evidence available (8,19). In this article, we investigate the nature of diffusion in crowded globular protein and random-coil polymer solutions that we take as a model system for diffusion in the intracellular environment, and show that protein diffusion strongly deviates from simple diffusion in these systems.

ANOMALOUS DIFFUSION

The description of the diffusion of a solute in a continuous medium is usually based on Fick's law, which defines the diffusion coefficient, D, of the solute in the media. Combined with conservation of matter, Fick's law leads to the diffusion equation, whose solution yields the usual expression for the mean-square displacement of a diffusing particle in three dimensions:

$$\langle r^2(t)\rangle = 6Dt, \tag{1}$$

which is characteristic of simple diffusion. The dependence of D on the diffusing particle's hydrodynamic radius and on the solvent viscosity is captured in the Stokes-Einstein equation. However, whereas Fick's law is an established phenomenological law for diffusion in isotropic fluids, there is no physical reason why it should always apply to more complex systems (20). More generally, in complex media, one might expect the mean-square displacement to obey a power law:

$$\langle r^2(t)\rangle = 6\Gamma t^{\alpha}, \tag{2}$$

Submitted August 10, 2004, and accepted for publication August 3, 2005.

Address reprint requests to Cécile Fradin, E-mail: fradin@physics.mcmaster.ca.

0006-3495/05/11/2960/12 $2.00

doi: 10.1529/biophysj.104.051078

where Γ is a constant that does not depend on time. If the exponent α is different from 1, then the diffusion is said to be anomalous, and if $\alpha < 1$ it is said to be subdiffusive. The quantity $\langle r^2 \rangle / 6t$ may still be defined as the apparent diffusion coefficient $D(t)$, but it will depend on the timescale, or equivalently on the length scale of the measurements:

$$D(t) = \Gamma t^{\alpha - 1}. \quad (3)$$

In fractal media, where there is no characteristic length scale, true anomalous diffusion is expected at all scales (21,22). Many physical systems, however, possess a characteristic length scale ξ, or a range of characteristic length scales. For example, in crowded solutions ξ is determined by various parameters such as the size of the solutes and the range of the pair correlation function (23). In general, when $\langle r^2 \rangle \ll \xi^2$ diffusion should be simple and correspond to diffusion in the fluid without obstacles. When $\langle r^2 \rangle \gg \xi^2$ diffusion should also be simple but correspond to diffusion in the composite medium. But when $\langle r^2 \rangle \approx \xi^2$, diffusion has to be anomalous to bridge these two regimes (24). This simple phenomenological argument does not predict pure anomalous diffusion, but just subdiffusion over an intermediary range of timescales. This type of crossover effect is well illustrated in Monte Carlo simulations of diffusion in the presence of immobile point obstacles (25).

ANOMALOUS DIFFUSION IN CELLS

Although observations of anomalous protein diffusion in cells have been reported (26–29), in the majority of studies to date, three-dimensional (3-D) cellular diffusion has been assumed to be simple. One reason for this is that, whereas two-dimensional membrane diffusion has been clearly shown to be anomalous (24,30,31), a fact sometimes attributed to corralling effects or to interactions with immobile membrane proteins acting as fixed obstacles, in the cytoplasm or the nucleus the case for anomalous diffusion of proteins is not easy to demonstrate, because diffusing proteins are too fast to be easily followed by single-particle tracking. With other experimental methods such as fluorescence recovery after photobleaching and fluorescence correlation spectroscopy (FCS), many artifacts have to be accounted for before the conclusion can be made that diffusion is anomalous, including: fluorophore blinking (29,32), reversible photobleaching (33), restriction of diffusion by membranes (34,35), and division of the population of tracers in several subspecies with different diffusion coefficients (29). As well, in our experience the aspect ratio of the experimental detection volume must be very accurately determined if one wants to study deviations from simple diffusion with FCS, because using an artificially high value of that parameter may conceal the real anomality of the diffusion if $\alpha > 0.9$. In one of the rare studies that considered anomalous diffusion of proteins inside cells, anomalous exponents in the range 0.7–1 were found, depending on the position within the cell (far from membranes), with smaller exponents consistently found in the nucleus (29). However, the authors showed that the data could be analyzed as well using a two-component model. In another study considering the anomalous diffusion of dextran polymers inside HeLa cells, anomalous exponents ranged from 0.7 to 0.9 (27). However, most of the evidence for 3-D anomalous protein diffusion in cells is in fact indirect.

Groups that have studied diffusion in cells report widely disparate data: the diffusion coefficients of tracer particles in cells are found to lie anywhere between 0 and 80% of their value in aqueous solution (29,33,36–43), reflecting the fact that the observed reduction in mobility depends on many variables. A tracer's mobility depends on which cell type (41), on which cell (33), but also on which position inside the cell (29) is selected for the study. The relative mobility of a tracer in a cell compared to an aqueous solution, D_{cell}/D_{aq}, has been shown to decrease with increasing size of the diffusing particles (37–39), which is an indirect indication that simple diffusion models may not apply and that diffusion might be anomalous. Possible interactions of the tracer particle with its environment also play a role (44). Finally, it seems that results might depend on the technique used (41), another possible indication that analysis of experimental data based on a simple diffusion model is misleading. A timescale-dependent $D(t)$ may explain some of the disparate data.

In this article, we report our studies as to whether the diffusion of proteins in the presence of molecular crowding due to other solutes is anomalous, a possibility that had not yet been investigated experimentally. We chose to focus on model systems where molecular crowding is provided by controlled concentrations of inert random-coil polymer molecules or globular proteins, thus reproducing the crowded conditions present in cells while reducing the risk of misinterpreting the experimental data. We used FCS to extract the anomalous diffusion exponent α corresponding to the diffusion of the proteins. The length scale of FCS measurements is set by the 0.5-μm diameter confocal detection volume and is relevant to the length scale of diffusion in the intracellular medium.

MATERIALS AND METHODS

Tracer particles and obstacles

Our samples were composed of a small concentration (typically 20 nM) of fluorescent tracer particles diffusing in an aqueous buffer (phosphate buffered saline (PBS)) in which obstacles were dissolved at a concentration up to 400 g/l. We used Dulbecco's PBS without magnesium and calcium: 137 mM NaCl, 15 mM Na_2HPO_4, 2.7 mM KCl, 1.5 mM KH_2PO_4, pH 7.4. The molecules used as obstacles were bovine serum albumin ((BSA) 66 kDa, Bioshop, Burlington, Ontario, Canada), streptavidin (52.8 kDa, Sigma-Aldrich, St Louis, MO), and dextrans (also from Sigma-Aldrich). The peak molecular weight values M_p, and polydispersity indices (M_n/M_w) of the dextrans used, as well as their approximate radii of gyration (R_g) and approximate overlap volume fractions (ϕ^*) in aqueous solution are shown in Table 1. The molecular weight values are reported as given by the supplier, and the values

TABLE 1 Characteristics of the dextrans used as obstacles

M_p (kDa)	M_n (kDa)	M_w(kDa)	M_w/M_n	R_g (nm)	ϕ^*
1.1	1.0	1.3	1.26	0.82	0.49
4.4	3.3	5.2	1.60	1.7	0.22
9.9	8.1	11.6	1.43	2.6	0.14
43.5	35.6	48.6	1.37	5.8	0.055
276.5	236.3	409.8	1.73	17	0.014
401.3	332.8	667.8	2.01	22	0.009

M_p, M_n, M_w are the peak value, number average, and weight average of the molecular mass, respectively. M_w/M_n is the polydispersity index. R_g is the radius of gyration and ϕ^* is the overlap volume fraction in aqueous solution, approximated as explained in the text.

of R_g were estimated from the molecular weight data using an experimental relationship from the literature (45). The values of ϕ^* were calculated following an approximate method (Schaefer, 1984) that divides the volume occupied by the monomers of a chain by an approximate expression for the pervaded volume of a chain: $\phi* = (M_p x/N_A)/((4/3)\pi R_g^3)$, where $x = 0.625\text{cm}^3/\text{g}$ is the specific volume of dextran (46) and N_A is Avogadro's number. The fluorescent tracers used in this study were streptavidin labeled with Alexa Fluor 488 (52.8 kDa, Molecular Probes, Eugene, OR), enhanced green fluorescent protein ((EGFP) 27 kDa, BD Biosciences Clontech, San Jose, CA), fluorescein, and FITC-dextran (282 kDa, Sigma-Aldrich). All molecules were used without further purification. They were dissolved at high concentrations with stirring as needed. The tracer molecules were selected for their absence of known interaction with the chosen obstacles and, except for the dextran, for their perfect monodispersity. To characterize the size of a tracer, its hydrodynamic radius R_H can be calculated from its diffusion coefficient using the Stokes-Einstein relation. The diffusion coefficients of EGFP, streptavidin, and FITC-dextran in the aqueous buffer in the absence of obstacles were measured by FCS and their hydrodynamic radii in the absence of obstacles were found to be 3.3, 4.9, and 9.5 nm respectively. The hydrodynamic radius of fluorescein can be estimated to be 0.8 nm from its known diffusion coefficient $D = 260\ \mu\text{m}^2/\text{s}$. The isoelectric point of streptavidin is $pI = 6.3$ (47), whereas that of EGFP is $pI = 5.5$ (48), meaning that in the pH = 7.4 buffer used both proteins are negatively charged. The use of charged proteins reduces the risks of aggregation, which are higher in crowded solutions due to the presence of depletion interactions.

Fluorescence correlation spectroscopy

FCS is a method relying on the detection and temporal analysis of the fluorescence signal emitted from a small confocal detection volume (49–52). Our homebuilt FCS setup is based on an inverted Nikon Eclipse TE2000-U microscope (Nikon, Tokyo, Japan). Fluorescence is excited by an argon ion laser (Melles Griot, Carlsbad, CA) whose 488-nm wavelength is selected by an excitation filter (HQ480/40×, Chroma Technology, Brattleboro, VT). The beam is focused in the sample by a water immersion objective (Plan Apo 60×, N.A. 1.20, Nikon). The output power of the laser is attenuated by neutral density filters and polarizers to obtain a radiant exposure at the focus in the range of 1–10 kW/cm^2. The emitted fluorescence collected by the objective passes through a dichroic mirror (Q505LP, Chroma), is filtered by an emission filter (HQ535/50m, Chroma), and focused through either a 30- or a 75-μm-diameter pinhole (Thorlabs, Newton, NJ) depending on the diameter of the beam entering the objective. The signal is detected by a photomultiplier (H7421, Hamamatsu Photonics, Shimokanzo, Japan) and fed into a multi-tau correlator (Flex01–08 ns, Correlator.com, Bridgewater, NJ) that computes its autocorrelation function. Autocorrelation functions were typically recorded for durations of 2–3 min and the measurements repeated 10–30 times for each sample. Analyses of the measured autocorrelation functions were performed using the software KaleidaGraph (Synergy Software, Reading, PA) that relies on the Levenberg-Marquardt algorithm. The exact dimensions of the confocal detection volume were evaluated before each experiment by fitting the autocorrelation function obtained from the free diffusion of fluorescein in PBS assuming $D = 260\ \mu\text{m}^2/\text{s}$ (53). Typical values obtained for the $1/e^2$ half-width of the detection volume were $w_0 = 220$ nm and $w_0 = 350$ nm for the two different pinhole sizes used. Most of the measurements were done at room temperature, but when necessary the temperature of the sample was controlled using both an inverted Peltier stage heater (PE100-NI, Linkam Scientific, Surrey, UK) and a custom-made Peltier objective heater (also from Linkam Scientific).

Analysis of the autocorrelation functions

Autocorrelation functions were analyzed using an expression modified to account for the possibility of anomalous diffusion. In this case, because the mean-square displacement follows a power law, $\langle r(t)^2\rangle \sim t^\alpha$, the expression of the autocorrelation function can be expected to be (54):

$$G(t) = \frac{1/N}{\left(1+\left(\frac{t}{\tau_D}\right)^\alpha\right)\left(1+\frac{1}{S^2}\left(\frac{t}{\tau_D}\right)^\alpha\right)^{1/2}}\cdot\left(1+\frac{T}{1-T}-e^{\frac{t}{\tau_T}}\right). \tag{4}$$

S is the aspect ratio, height to width, of the ellipsoidal detection volume. N is the average number of fluorophores and τ_D their characteristic residence time in this volume; τ_D is related to the apparent diffusion coefficient D of the fluorophores and to the half-width w_0 of the detection volume:

$$\tau_D = \frac{w_0^2}{4D}. \tag{5}$$

The second term in Eq. 4 accounts for the existence of a nonfluorescent triplet state (55): τ_T is the relaxation time of the triplet state, and T is the average fraction of fluorophores found in the triplet state. The simple analytical equation given in Eq. 4 was derived using one of several possible diffusion equations leading to anomalous diffusion, and hence is not necessarily an exact solution for all cases of anomalous transport. However, it has been shown to be a very good approximation of the more complex solution of a larger class of anomalous diffusion equations (27). Importantly, the asymptotic behavior of the autocorrelation function depends only on the probability of a particle to return to the origin, which is independent of the anomalous diffusion model used (56). Both the triplet state relaxation time, τ_T, and the aspect ratio, S, were fixed in the fitting process for all the samples containing obstacles. The value of these two parameters was determined by fitting autocorrelation functions measured for the diffusion of the tracer in an aqueous solution immediately before performing the experiments in the presence of molecular crowding. In the case of EGFP, τ_T is the decay time of the fast protonation process that causes fluorophore blinking, whereas the blinking due to the slow protonation process is not expected to occur at the pH used in this study (32). Indeed, Eq. 4 with $x = 1$ fits the autocorrelation data well for diffusion of EGFP in PBS without obstacles.

In the case where $\alpha = 1$, diffusion is simple and the diffusion coefficient D calculated from the measured value of τ_D using Eq. 5 is a constant, as defined in Eq. 1. On the other hand, when $\alpha \neq 1$ diffusion is anomalous and the diffusion coefficient D calculated using Eq. 5 is just an apparent diffusion coefficient, describing diffusion at the length scale w_0 set by the experiment, or equivalently at the timescale τ_D. As defined in Eqs. 2 and 3, the apparent diffusion coefficient is:

$$D(\tau_D) = \Gamma\,\tau_D^{\alpha-1}. \tag{6}$$

Multicomponent models are often used to explain deviations from simple diffusion. The corresponding expression of the diffusion term of the autocorrelation function for such models is:

$$G(\tau) = \sum_{i=1}^{n}\frac{a_i}{\left(1+\frac{\tau}{\tau_{Di}}\right)\left(1+\frac{1}{S^2}\left(\frac{\tau}{\tau_{Di}}\right)\right)^{1/2}}, \tag{7}$$

where a_i is the contribution of the ith component to the total amplitude of the autocorrelation function, $G(0)$, and τ_{Di} is the characteristic residence time of this component. To assess the validity of using an anomalous diffusion model as opposed to a multiple-component model, the autocorrelation functions were analyzed both using a two-component model (Eq. 7 with $n = 2$), where it is assumed that two different fluorescent species are diffusing normally in solution (29), and using a maximum entropy method adapted for FCS (MEMFCS), where it is assumed that a large number of different fluorescent species are diffusing normally in solution (Eq. 7 with $n = 100$), each with a different diffusion coefficient (57,58). We used the MEMFCS algorithm recently made available by Sengupta and colleagues (57) based on the maximum entropy method of Skilling and Bryan (59). Like other fitting algorithms, MEMFCS seeks to minimize the chi-square parameter χ^2 describing the distribution of the residuals, but MEM algorithms also seek to maximize an entropy-like quantity, $S = -\sum_i p_i \ln p_i$, where $p_i = a_i/\sum_j a_j$ for FCS. Maximizing entropy results in the maximally wide distribution of τ_{Di} values that is consistent with the data.

Autocorrelation data showing obvious signs of the passage of large fluorescent aggregates through the detection volume during the measurement, both by erratic deviations from a smooth decay in the 0.1–10-s time range and the presence of spikes in the photon count history recorded by the correlator at a resolution of 67 ms were rejected. In contrast to the discarded measurements showing evidence of aggregation, the measurements retained for analysis were highly reproducible and independent from protein preparation. The occurrence of aggregates varied considerably from one protein batch to the next, implying that aggregation is not an intrinsic property of the system, but suggesting instead that aggregates are formed around impurities. The number of aggregation occurrences became more frequent at very high concentrations of high molecular weight dextrans, and up to two-thirds of the curves had to be rejected. However, ultracentrifugation of our samples up to 200,000 × g using a Beckman TL-100 Tabletop Ultracentrifuge (Beckman Coulter, Fullerton, CA) greatly reduced the frequency of the aggregation occurrences. But the anomalous diffusion exponent and the diffusion coefficient measured did not change after ultracentrifugation.

RESULTS

Two different types of diffusion behavior were obtained depending on the presence or absence of obstacles in the buffer, as illustrated by the autocorrelation curves presented in Fig. 1. In samples containing only very low concentrations of solutes, the resultant diffusion cannot be distinguished from simple diffusion. The simple diffusion model for a single species in solution (Eq. 4 with $\alpha = 1$) is very successful in fitting the correlation data for such systems. However, in crowded solutions, this simple equation no longer fits the data. The autocorrelation data show a broadening in the decay at timescales corresponding to diffusion (Fig. 1), indicating a wider distribution of diffusion times of the tracer through the detection volume.

Two models frequently used to model the diffusion of tracers in living cells are the two-component model (Eq. 7 with $n = 2$) and the anomalous diffusion model (Eq. 4), as described in Materials and Methods. For the crowded solution, the fit obtained using the anomalous diffusion model is shown in Fig. 1 *a*, whereas Fig. 1 *b* compares the residuals of the fits for both models, showing that the anomalous diffusion model gives a slightly better match. Another way to distinguish between these two models is to examine the long-time behavior of the autocorrelation data. Although multi-tau correlators may introduce errors at long times for oscillatory signals (60), the signal considered here is not oscillatory, and thus the long-time behavior of the correlation data should be reliable. At timescales above the characteristic average residence time, the autocorrelation function of multicomponent models scales as $t^{-3/2}$ (Eq. 7), whereas in the anomalous diffusion model, the autocorrelation function scales as $t^{-3\alpha/2}$ (Eq. 4). As shown in Fig. 1 *c*, the asymptotic behavior of the autocorrelation function corresponding to the diffusion of streptavidin in the absence of dextran obstacles is identical to that predicted by the simple diffusion model. But when dextran obstacles are present, it clearly deviates from the $t^{-3/2}$ scaling predicted by multicomponent models. On the contrary, in the latter case, it is well described by the $t^{-3\alpha/2}$ scaling predicted by the anomalous model. Finally, the fact that the same exponent $\alpha = 0.76$ describes equally well short-time behavior around τ_D and the asymptotic behavior above τ_D indicates that the diffusion may be consistently anomalous over a large time range.

We used the MEMFCS fitting algorithm to further test the agreements of the two models with the experimental data, and to validate the use of the anomalous diffusion model to analyze our data. Fig. 2 shows the effective distributions in average residence times calculated using the MEMFCS software that correspond to the autocorrelation data shown in Fig. 1 *a*. Although diffusion in the absence of obstacles yields a narrow distribution, as expected (57), diffusion in the presence of obstacles produces a wide distribution with a distinct tail at long times. Such a distribution is not compatible with a two-component model. Indeed, if we apply the MEMFCS algorithm to simulated autocorrelation data generated using the equation for the two-component model (Eq. 7 with $n = 2$ where the parameters were obtained by fitting the experimental data shown in Fig. 1), then we find a distribution with two narrow peaks centered around the characteristic residence time of the two species (cf. Fig. 2). The presence of two clearly separated peaks is not due to the use of simulated autocorrelation data. The maximum entropy method has been shown to be able to separate the contributions of two different species in different real two-component samples (58,61). The failure of the two-component model to predict the correct distribution of residence times proves that the complex behavior of the systems under study cannot be reduced to coexistence of two distinct tracer populations.

In contrast, if the MEMFCS algorithm is applied to simulated autocorrelation data generated using the anomalous diffusion model, then we find a wide and asymmetric distribution of residence times nearly identical to the distribution obtained from the experimental data (cf. Fig. 2). The experimental distribution is in good agreement with a subdiffusive behavior of the fluorescent tracer particles, and we found this agreement to hold for all concentrations of obstacles. A wide distribution of diffusion times is expected in the case of anomalous diffusion, as shown by applying the

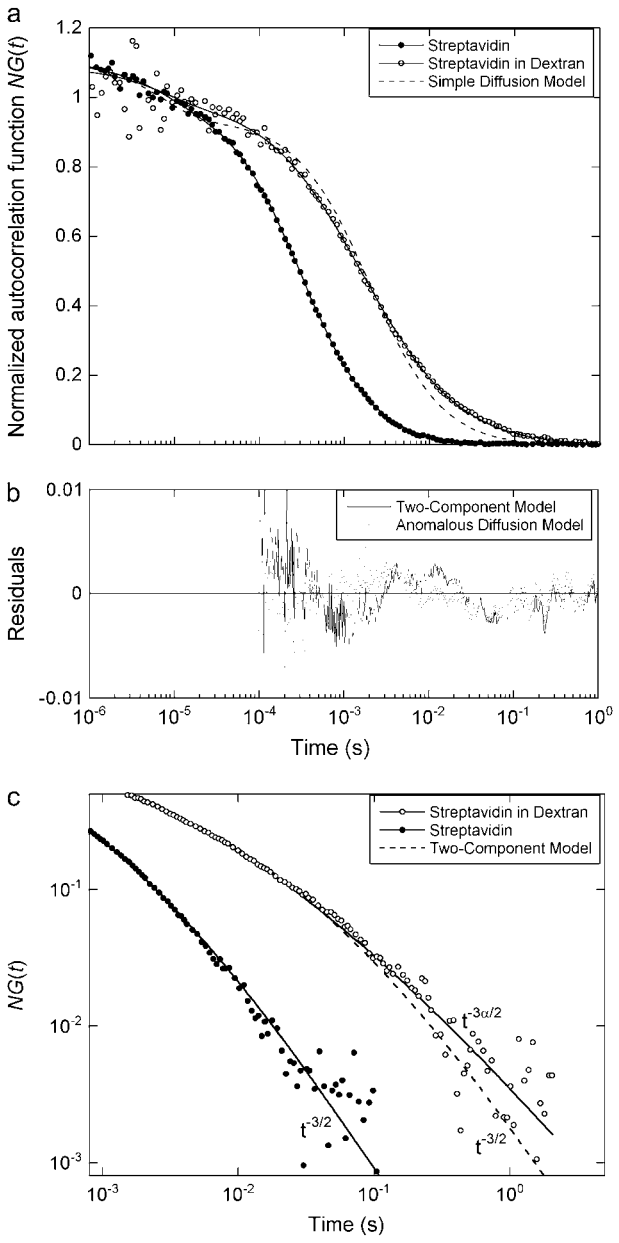

FIGURE 1 Normalized autocorrelation functions for streptavidin diffusing in PBS buffer with and without dextran obstacles (200 g/l of 276.5 kDa dextran). The fit of these autocorrelation functions using the anomalous diffusion model (Eq. 4) gives $\alpha = 0.99 \pm 0.01$ for no obstacles, and $\alpha = 0.76 \pm 0.01$ with obstacles (*solid lines*). The failure of the fit with the simple diffusion model (Eq. 4 with $\alpha = 1$) for the case with obstacles is also shown (*dashed line*). The fit with the two-component model (Eq. 7) closely resembles the fit with the anomalous diffusion model and is not shown for clarity of the plot. (*b*) Residuals of the fits of the autocorrelation function in panel *a* for the case with dextran obstacles with both the anomalous diffusion model (dots, $\chi^2 = 0.0024$ for 459 data points from $t = 0.5$ μs to 1 s, with three adjustable parameters) and the two-component model (*solid line*, $\chi^2 = 0.0028$ for the same data points with four adjustable parameters) are shown for the timescale relevant to diffusion. At shorter timescales, the two models are practically identical and the scatter in the data is large. (*c*) Asymptotic long-time behavior of the data and fits to the autocorrelation functions shown in panel *a*. For the case without dextran obstacles, the fit with the anomalous diffusion model shows a $t^{-3/2}$ scaling (*solid line*). For the case with obstacles, the fit with the anomalous diffusion model shows a $t^{-3\alpha/2}$ scaling (*solid line*, $\alpha = 0.76$), whereas the fit with the two-component model shows a $t^{-3/2}$ scaling (*dashed line*).

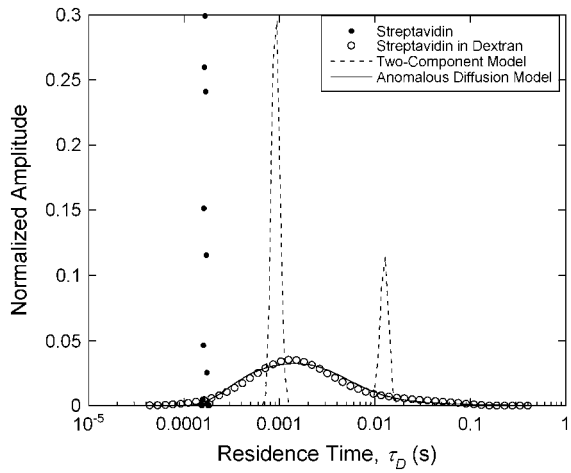

FIGURE 2 Effective distributions in average residence times calculated with the MEMFCS algorithm for the experimental autocorrelation data shown in Fig. 1 *a* (*symbols*), and for two sets of simulated autocorrelation data corresponding to the case of streptavidin diffusing in 200 g/l 276 kDa dextran. The first set was generated using the anomalous diffusion model and the parameters found from the fit of the experimental data ($\alpha = 0.76$, $\tau_D = 1.6$ ms) and the second set was generated using the two-component model and the parameters found from the fit of the experimental data ($\tau_{D1} = 0.90$ ms, $\tau_{D2} = 12$ ms, relative amplitude $a_2/a_1 = 0.41$), as explained in the text. The peak values of the distributions found by the MEMFCS algorithm for the two-component model are 0.94 and 13 ms.

maximum entropy method to simulated fluorescence recovery after photobleaching experiments (53). Also, long-tail kinetics, which will result in an asymmetric distribution of diffusion times, were predicted as a result of anomalous diffusion (62). The MEMFCS analysis does not distinguish between a single component diffusing anomalously and a continuous distribution of components diffusing normally having coincidentally the same distribution of residence times. However, if the diffusion in our samples were not actually anomalous, then the distribution produced by the MEMFCS algorithm from the experimental data could have been incompatible with anomalous diffusion. But because the distributions do agree, even if the diffusion is not in fact anomalous, we can characterize the experimental distribution using only the two parameters $D(\tau_D)$ and α extracted from the anomalous diffusion model, which determine the center and the width of the distribution. For the above reasons, we discuss our results using the anomalous diffusion model throughout the rest of this article.

The apparent diffusion coefficient $D(\tau_D)$ obtained using the anomalous diffusion model for streptavidin in the presence of various concentrations of dextrans of different molecular weight is shown in Fig. 3 *a*. For streptavidin, $D(\tau_D)$ is found to decrease with increasing concentration of

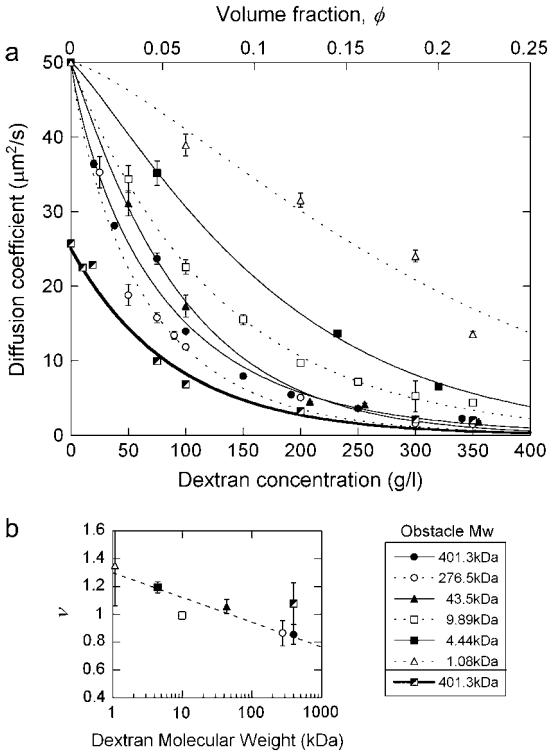

FIGURE 3 (*a*) Apparent diffusion coefficient, $D(\tau_D)$, associated with the diffusion of streptavidin as a function of dextran concentration for dextrans of various average molecular weights (*open* and *solid symbols*). Also shown is $D(\tau_D)$ for a 282 kDa dextran diffusing in a solution crowded by a 401.3 kDa dextran (*half-solid symbols*). Lines represent stretched exponential fits as explained in the text. Where necessary, some of the data points have been slightly shifted horizontally for clarity of the plot. (*b*) Value of the exponent ν as a function of the molecular weight of the polymers used as obstacle. The dotted line is a guide for the eyes.

dextran as predicted by all models describing the diffusion of spherical tracer particles in the presence of macromolecular crowding (8,13,19) and as previously observed in similar systems (63). Our data in Fig. 3 *a* can be satisfactorily fitted by a stretched exponential:

$$\frac{D}{D_0} = e^{-\beta\phi^{\nu}}, \tag{8}$$

where D_0 is the diffusion coefficient of the tracer particle in aqueous solution, ϕ is the polymer volume fraction, and β and ν are scaling parameters. Equation 8 corresponds to the prediction made by several models describing the diffusion of globular tracer particles in polymer solutions. All these models rely to some extent on phenomenological arguments, and the physical significance of the coefficients β and ν is not well defined (8). Some models predict different constant values for ν (64), whereas Phillies' model predicts a dependence on molecular weight (65). In our case we observe no clear trend in β as a function of the polymer molecular weight, and find that ν drops from 1.35 to 0.85 as the polymer molecular weight increases (cf. Fig. 3 *b*).

However, the novel and surprising result of our study is that the diffusion of streptavidin is anomalous in the presence of dextran. The data in Fig. 4 *a* show two trends with respect to the anomalous exponent. First, α drops with increasing dextran concentration until it reaches a limit value $\alpha_1 \approx 0.74$ for the large molecular weight dextrans. In the cases of the smaller dextran obstacles, only the decay regime is observable. Second, the initial decay of the anomalous exponent becomes steeper with increasing molecular weight of the obstacles. The fits indicated in Fig. 4 *a* have been made assuming an asymptotic exponential decay to a limit value α_1 common for all dextrans:

$$\alpha = \alpha_1 + (1 - \alpha_1)e^{-\phi/\phi_0}, \tag{9}$$

where α_1 was estimated first by fitting the curves in Fig. 3 *a* for the three highest molecular weight dextrans allowing α_1 to vary. We found $\alpha_1 = 0.74 \pm 0.02$. Then all curves were fitted using this limit value. The origin and value of α_1 are discussed below. Fig. 4 *b* shows the value of ϕ_0 as a function of the polymer molecular weight.

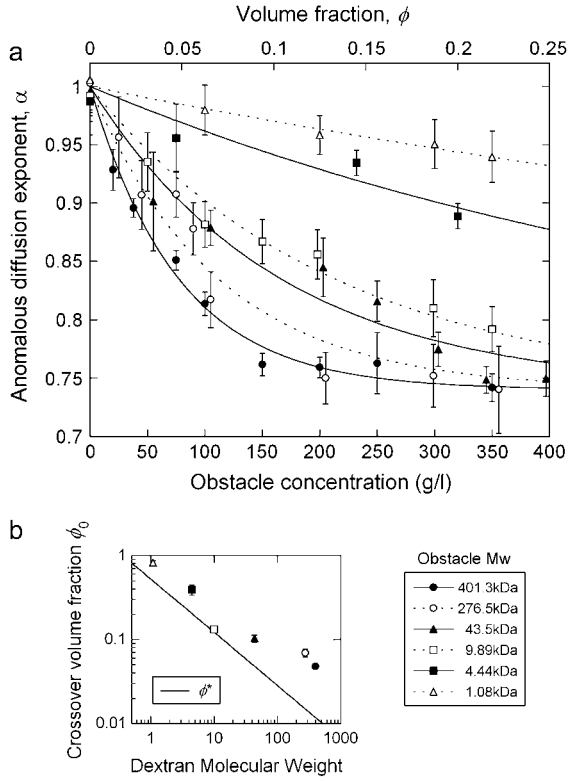

FIGURE 4 (*a*) Anomalous diffusion exponent associated with the diffusion of streptavidin as a function of obstacle concentration for dextrans of various average molecular weights. Lines are fits to the data using Eq. 10 with $\alpha_1 = 0.74$. Where necessary, some of the data points have been slightly shifted horizontally for clarity of the plots. (*b*) Crossover volume fraction ϕ_0 found as a result of the fit shown in panel *a* for the different dextrans used as obstacles. The solid line shows the overlap volume fraction ϕ^* calculated as explained in Materials and Methods.

To test for an effect of the negative charge of streptavidin on the diffusion, we modified the ionic strength of the buffer solution by increasing the NaCl concentration in our samples to screen the interactions due to the charges on the streptavidin. As shown in Fig. 5, adding up to 1 M NaCl to the PBS buffer has no effect on the anomalous diffusion exponent α, with or without dextran crowding. Above a 1-M concentration of salt in the sample containing 200 g/l of the 276 kDa dextran, there is an increase in the rate of aggregation as evidenced by spikes in the photon count history and corresponding correlations at long times. This is due to the well-known salting out effect: proteins start aggregating upon screening of their electrostatic charges. As expected, aggregation is enhanced by the presence of the dextran, which induces attractive depletion interactions between the proteins. In the control samples not containing dextran, the presence of aggregates was not detected even at the highest salt concentrations used (5 M). For the samples containing dextran, the error introduced by the presence of aggregates reduces the measured value of α as shown above 1 M salt. And above 2 M, the aggregations become too frequent to admit a fit of the data with the anomalous diffusion model. We also observed that the apparent diffusion coefficient is independent of ionic strength (data not shown).

We tested for a temperature dependence of the subdiffusive behavior within a biologically relevant range, from 15 to 45°C. The experiment was done for streptavidin diffusing in samples containing either 75 g/l or 200 g/l of the 276 kDa dextran. Results are shown in Fig. 6. Although the apparent diffusion coefficient increases with increasing temperatures as expected from the change in the buffer viscosity, the anomalous exponent α is remarkably constant in both cases, showing that temperature changes in this temperature window do not strongly affect the anomalous nature of the diffusion.

To assess whether the anomalous behavior would depend on the nature of the tracers used, we repeated this experiment with different tracers. As shown in Fig. 7, the diffusion of the other globular protein used as a tracer, EGFP, is anomalous to a degree comparable to that of streptavidin. On the other hand, for fluorescein, the diffusion is normal within experimental errors. For the large dextran tested, the diffusion is also observed to be normal or only slightly anomalous, suggesting that the rules governing the self-diffusion of the polymer obstacles are quite different from those governing the diffusion of the globular tracers.

Finally, to check whether the effect we observe in random-coil polymer solutions is in fact relevant to the diffusion of proteins in the cytoplasm of cells, where molecular crowding

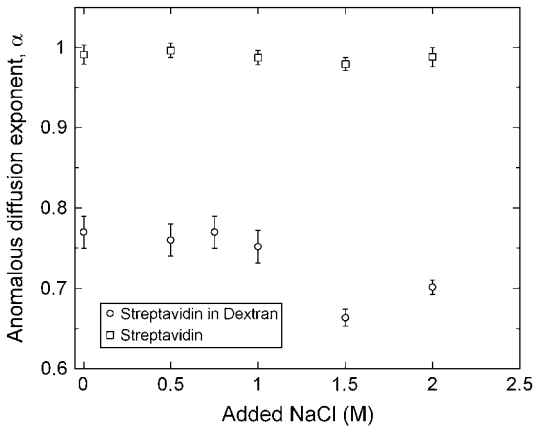

FIGURE 5 Anomalous diffusion exponent corresponding to the diffusion of streptavidin in PBS with and without 200 g/l of 276 kDa dextran, as a function of added NaCl.

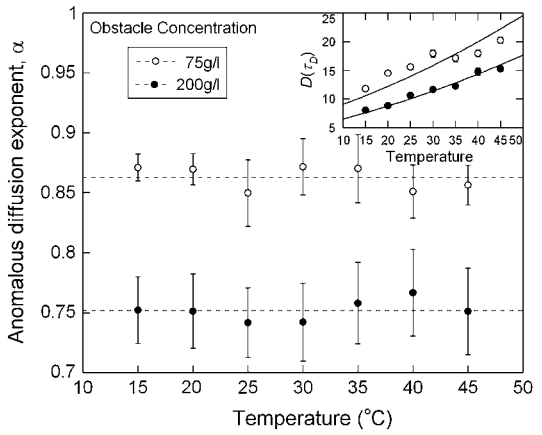

FIGURE 6 Anomalous diffusion exponent α associated with the diffusion of streptavidin in presence of 75 g/l and 200 g/l of 276 kDa dextran as a function of the temperature. The average values of the anomalous diffusion exponent α over the considered temperature range are shown: $\alpha = 0.86 \pm 0.01$ and 0.75 ± 0.01. The inset shows the corresponding variation of the apparent diffusion coefficient $D(\tau_D)$ in $\mu m^2/s$, and the lines are fits assuming that the temperature dependence is only due to the change in the viscosity of water.

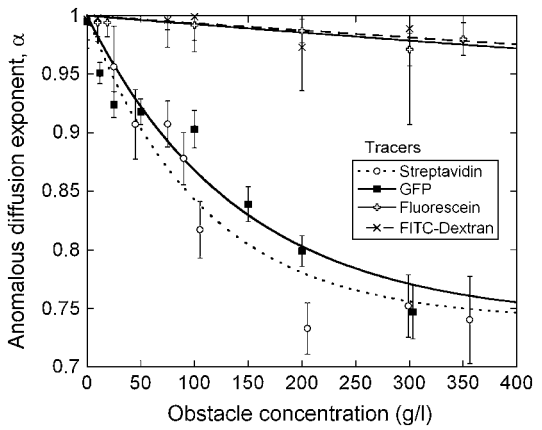

FIGURE 7 Anomalous diffusion exponent as a function of dextran concentration fitted to Eq. 10 for various tracers: EGFP and streptavidin in solutions crowded with the 276.5 kDa dextran, and fluorescein and 282 kDa FITC-dextran in solutions crowded with 401.3 kDa dextrans. Where necessary, some of the data points have been slightly shifted horizontally for clarity of the plots.

is mainly due to high protein concentrations, we used other proteins as obstacles. We investigated the diffusion of streptavidin against very high concentrations of bovine serum albumin, a globular protein of comparable molecular weight, and against high concentrations of unlabeled streptavidin. Results are shown in Fig. 8. At a 350 g/l concentration of BSA, the exponent α corresponding to the diffusion of streptavidin is 0.91 ± 0.02. Thus, the subdiffusive behavior is considerably weaker than that observed in the case of the large dextrans, but comparable to that obtained in the case of the smaller dextrans. In the case where streptavidin (not fluorescently labeled) was used as an obstacle, behavior more anomalous than in the case of BSA was observed up to ~130 g/l. However, comparison could not be made at higher concentrations due to the lower solubility of streptavidin in PBS. The observation that streptavidin can cause the subdiffusion of labeled streptavidin molecules is nevertheless significant, because it indicates that anomalous diffusion can occur in these systems in the absence of depletion interactions.

DISCUSSION

Anomalous diffusion has been previously observed and explained in a variety of nonbiological systems (56). Subdiffusion is expected either in the presence of a high concentration of fixed obstacles or in the presence of a distribution of binding sites, as was shown by Monte Carlo simulations of random walks (25,66,67). In fractal systems, the value of α depends on the type of fractal. For site percolation at the percolation threshold, numerical methods show that $\alpha = 0.53$ in 3-D (22). Experimentally, subdiffusion has been unambiguously observed in cross-linked polymer networks where the centers-of-mass of the obstacles are fixed (68–71). The variety of anomalous exponents measured in these networks were explained by the existence of different effects in addition to the excluded volume effects considered in the simulations: coupling of the tracer motion with the fluctuations of the network filaments (69), trapping (70), and interactions with the obstacles (71).

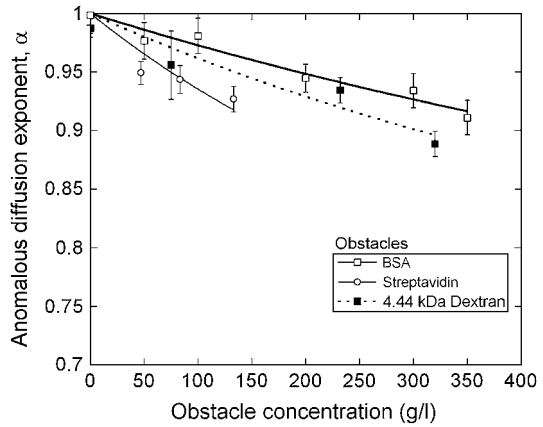

FIGURE 8 Anomalous diffusion exponents associated with the diffusion of streptavidin in solutions crowded with either BSA or nonfluorescent streptavidin for different concentrations of the obstacle proteins fitted to Eq. 10. For comparison, the exponent associated with diffusion in a solution crowded with a 4.44 kDa is also indicated.

But in the experiments presented here, the obstacles causing the anomalous diffusion are mobile, and have a mobility comparable to that of the tracer proteins (cf. Fig. 3 for the diffusion of the 282 kDa dextran). This is an unexpected result because for diffusing point obstacles interacting with a point tracer through excluded volume effects, simulations either do not show anomalous diffusion (25), or they show anomalous diffusion only at very short timescales (72). Furthermore, some groups have measured the diffusion of tracers in solutions crowded with mobile random-coiled polymers or globular proteins without observing or reporting this diffusion to be anomalous (73–77). However, our experiments and analysis show very clearly otherwise. One reason for this apparent discrepancy is that subdiffusion does not seem to appear or is very weak, as we show here, for small tracer particles such as fluorescein or for random-coil polymer tracers such as dextran, and most studies to date have been concentrating on the behavior of such tracers (74,76). Other studies have been restricted to low polymer concentrations (77), where the effect is slight and can easily be missed, because it can be incorrectly attributed to the artifacts mentioned in the introduction. In support of our observation that diffusion of tracer particles is anomalous in polymer solutions, it has very recently been shown using scale-dependent FCS measurements that the diffusion of dyes in polymer solutions was slightly anomalous (78). Furthermore, it was reported several times that the measured diffusion coefficients of proteins point to a difference between macroscopic and microscopic viscosities (10,73,77), which may result in anomalous diffusion at intermediate length scales for these proteins.

Although it is clear that the deviation from normal diffusion behavior has to arise from the heterogeneous nature of the solution and interactions between the tracer particle and the obstacles, the nature of these interactions and the mechanism by which they cause anomalous diffusion need to be resolved. The possibility that the distribution of residence times observed in crowded media (Fig. 2) reflects the presence of inhomogeneities due to depletion interactions cannot be entirely ruled out. However, several pieces of evidence speak against this scenario. First, when aggregates are removed by ultracentrifugation, the anomalous behavior observed does not change. Second, if inhomogeneities present in our samples were due to depletion interactions, we would expect them to grow larger upon screening of the negative charges of the tracer proteins. But when adding NaCl in the solution, there are no observable changes until ~1.5 M NaCl, when we start detecting signs of aggregation as a stable phenomenon. This suggests that for solutions with no added NaCl, aggregation is a relatively rare occurrence.

Third, in homogeneous streptavidin solutions where depletion interactions disappear, we still observe that the diffusion of fluorescent streptavidin is anomalous, to a degree comparable to that of its diffusion in small dextrans. In addition to these observations, the lack of visible temperature dependence for the anomalous behavior speaks against depletion interactions being the single cause for subdiffusion. In fact, it speaks against all possible models in which entropy effects cause the anomalous behavior, as entropy driven interactions will be sensitive to temperature changes.

Another potential cause for the anomalous diffusion is the polydispersity of the obstacles. Indeed, it may be noted that the polydispersity index (PI) of the dextrans used in our experiments roughly correlates with their molecular weight, as can be seen in Table 1, and so the observed dependence of α on molecular weight could in fact be a dependence on PI. However, whereas the PI may play a role in determining the value of α, the key variable is certainly the molecular weight. Indeed, when we mix two dextran samples of same concentration but unequal average polymer weights to obtain a sample of increased PI but lower average molecular weight as compared to the highest molecular weight sample, the anomalous diffusion exponent α increases (data not shown). Also, diffusion is still anomalous when the solution is crowded with strictly monodisperse obstacles such as BSA or streptavidin.

We hypothesize that the subdiffusion process we observe may be separated into two different regimes, which correspond to two different anomalous diffusion mechanisms. These two different regimes are visible in Fig. 4 *a*, where the anomalous exponent α depends strongly on obstacle concentration below the crossover volume fraction ϕ_0 whereas it is constant above ϕ_0. The first regime corresponds to solutions containing globular proteins, low molecular weight dextrans, or high molecular weight dextrans at low concentration. The second regime corresponds to solutions containing high molecular weight dextrans at high concentrations. The crossover volume fraction ϕ_0 is found to be slightly above the chain overlap volume fraction ϕ^* for all dextrans (cf. Fig. 4 *b*).

In the first regime, our samples may be compared to colloidal systems, picturing both the tracers and obstacles as spheres. These systems are similar in that in both cases the tracers and obstacles are globular, comparable in size, and interact mainly through excluded volume or hydrodynamic interactions. Also, both systems are glass-forming solutions. Single particle tracking experiments in colloidal systems showed that anomalous diffusion could be attributed unambiguously to caging effects (79,80). The diffusion behaves according to the prediction of the two-phase model, where diffusion is anomalous only at timescales where both rattling within a cage and hopping out of a cage significantly contribute to displacement. Observations in our systems are compatible with transient caging of the tracer proteins by an ensemble of random-coil polymer molecules or globular proteins. First, neither dextran molecules that can move by means of reptation nor small fluorescein molecules are likely to be caged. Second, because larger polymers will move slower, they will tend to trap the tracer molecules for a longer time, causing the diffusion to be more anomalous. Third, compared to the case of globular proteins obstacles, anomalous diffusion is more pronounced in the case of random-coil polymer obstacles, because their more extended conformations increase the possibility of complex steric interactions and hence the probability of caging globular tracers. The smaller range of anomalous exponents we observe in this regime $\alpha \approx 0.9$–1 compared to those reported in the mentioned colloidal systems $\alpha \approx 0.1$–1 (81) could be attributed to the fact that our systems are farther away from the glass transition, which can be estimated using the Fox equation (82) to be above $\phi_g = 0.4$ for dextrans in water at room temperature. Alternatively, one could argue that, in this low concentration regime, transient inhomogeneities due to depletion interactions are the cause of the anomalous behavior we observe because they could act as traps for the tracer proteins. The tracers may associate with and dissociate from these inhomogeneities while diffusing through the detection volume, which may result in an anomalous diffusion behavior similar to that predicted by caging models, or by models where tracers are allowed to bind to obstacles (66).

In the second regime, which occurs well above the chain overlap volume fraction ϕ^*, that is, at a volume fraction where the polymer chains are entangled, we observe a constant value of the anomalous exponent $\alpha_1 = 0.74 \pm 0.02$. This value is reminiscent of the exponent $\alpha = 3/4$ measured for the diffusion of beads in cross-linked polymer networks when the tracer diameter is larger than the network mesh size in agarose gels (68) and in actin networks (69). The same behavior ($\alpha = 3/4$) has been observed for the diffusion of lipid granules in the cell cytoplasm (83), and recently for the diffusion of dextran in the cytoplasm of HeLa cells (27). In the case of the cross-linked networks, this result has been explained by a strong coupling between the diffusing beads and the thermal motions of the actin filaments, because the lateral mean-square displacement of the monomers of polymer filaments scales as $t^{3/4}$ at short times (69). In our system at high dextran concentration, the polymer chains form an entangled, but not cross-linked, network. The center-of-mass diffusion of the polymer is slow compared to the thermal fluctuations of the monomers such that we can expect the coupling between the tracer proteins and the segments of the chains to become the predominant relaxation mechanism for the tracers, resulting in a subdiffusion characterized by $\alpha = 3/4$, which is what we observe. Once the polymer chains are well entangled, the average mesh size of the network does not depend on the polymer molecular weight (84), so that the characteristics of the motion of tracer particles should not depend on it either. This is in agreement with our observations: well above ϕ^*, neither the apparent diffusion coefficient nor the anomalous exponent α depend on the molecular weight of the dextrans.

CONCLUSION

This study is the first report of unequivocal observations of anomalous diffusion of proteins in solutions crowded by mobile obstacles. Our results suggest that the failure of models of diffusion in random-coil polymer solutions to predict experimental observation, which becomes apparent at high concentrations, is due at least in part to the fact that none of these models allow for anomalous diffusion. Not only in random-coil polymer solutions, but also in cells, experimental measurements of protein diffusion, and models of processes that depend on diffusion should be done considering the possibility of anomalous diffusion. The cytoplasm may be pictured as a cytoskeleton filament network with a characteristic mesh size $\xi \approx 20$–30 nm (37,38) filled with an aqueous phase containing a very high concentration of proteins, up to 400 g/l (85,86). Because this network mesh size is too large to produce anomalous diffusion for typical-sized proteins, we expect that the slight anomalous diffusion observed in the cytoplasm (28,29) may be due to the cage rearrangement effect or to binding interactions. Indeed, it was shown that anomalous diffusion of dextrans in cell did not disappear after depolymerization of the microtubule network (27). The fact that diffusion should generally be expected to be anomalous in the cytoplasm, even if the effect is small, is significant because it means that diffusion coefficients measured at larger scales will lead to an underestimation of the mobility of the proteins at molecular scales. In addition, even a slightly anomalous behavior might influence the outcome of such processes as pattern formation, whose stability has sometimes been linked to subdiffusion of the reactants (87). Also, our study of diffusion of proteins at high random-coil polymer concentration reproduces conditions found in living systems: in bacterial films (88), in the periplasmic peptidoglycan network of Gram-negative bacteria, in the hyaluronic acid coat enveloping some eukaryotic cells (89), and in the chromatin in places where DNA is not wrapped around structural proteins. Indeed, the anomalous behavior observed in cell nuclei for EGFP (29) is consistent with a motion coupled with the thermal fluctuations of filaments (α approaches 3/4). Although the cellular environment is more complex than our simplified model systems, understanding diffusion in these systems will facilitate the use of probe diffusion to meaningfully characterize the cellular environment at the scale of biomolecules.

We thank Dr. Sudipta Maiti for graciously providing the MEMFCS algorithm and Kanchan Garai for support with using the software.

This work was funded by the Natural Sciences and Engineering Research Council (NSERC) of Canada. D.B. is the recipient of a CGS-M NSERC scholarship and C.F. is supported through the Canada Research Chairs Program.

REFERENCES

1. Pederson, T. 2000. Diffusional protein transport within the nucleus: a message in the medium. *Nat. Cell Biol.* 2:E73–E74.
2. Cluzel, P., M. Surette, and S. Leibler. 2000. An ultrasensitive bacterial motor revealed by monitoring signaling proteins in single cells. *Science.* 287:1652–1655.
3. Macnab, R. 2000. Action at a distance: bacterial flagellar assembly. *Science.* 290:2086–2087.
4. Guthold, M., X. Zhu, C. Rivetti, G. Yang, N. Thomson, S. Kasas, H. Hansma, B. Smith, P. Hansma, and C. Bustamante. 1999. Direct observation of one-dimensional diffusion and transcription by Escheria coli RNA polymerase. *Biophys. J.* 77:2284–2294.
5. Berry, H. 2002. Monte Carlo simulations of enzyme reactions in two dimensions: fractal kinetics and spatial segregation. *Biophys. J.* 83: 1891–1901.
6. Crick, F. 1970. Diffusion in embryogenesis. *Nature.* 225:420–422.
7. Valdez-Taubas, J., and H. Pelham. 2003. Slow diffusion of proteins in the yeast plasma membrane allows polarity to be maintained by endocytic cycling. *Curr. Biol.* 13:1636–1640.
8. Masaro, L., and X. X. Zhu. 1999. Physical models of diffusion for polymer solutions, gels and solids. *Prog. Polym. Sci.* 24:731–775.
9. Hall, D., and A. P. Minton. 2003. Macromolecular crowding: qualitative and semiquantitative successes, quantitative challenges. *Biochim. Biophys. Acta.* 1649:127–139.
10. Lavalette, D., C. Tetreau, M. Tourbez, and Y. Blouquit. 1999. Microscopic viscosity and rotational diffusion of proteins in a macromolecular environment. *Biophys. J.* 76:2744–2751.
11. Scott, R. A., and N. A. Peppas. 1999. Highly crosslinked, PEG-containing copolymers for sustained solute delivery. *Biomaterials.* 20:1371–1380.
12. Whang, K., T. K. Goldstick, and K. E. Healy. 2000. A biodegradable polymer scaffold for delivery of osteotropic factors. *Biomaterials.* 21:2545–2551.
13. Zimmerman, S., and A. Minton. 1993. Macromolecular crowding: biochemical, biophysical, and physiological consequences. *Annu. Rev. Biophys. Biomol. Struct.* 22:27–65.
14. Asakura, S., and F. Oosawa. 1958. Interaction between particles suspended in solutions of macromolecules. *J. Polym. Sci.* 33:183–192.
15. Minton, A. P. 2001. The influence of macromolecular crowding and macromolecular confinement on biochemical reactions in physiological media. *J. Biol. Chem.* 276:10577–10580.
16. Minton, A. P. 1993. Macromolecular crowding and molecular recognition. *J. Mol. Recognit.* 6:211–214.
17. Rivas, G., J. A. Fernandez, and A. P. Minton. 2001. Direct observation of the enhancement of noncooperative protein self-assembly by macromolecular crowding: indefinite linear self-association of bacterial cell division protein FtsZ. *Proc. Natl. Acad. Sci. USA.* 98:3150–3155.
18. Sasahara, K., P. McPhie, and A. P. Minton. 2003. Effect of dextran on protein stability and conformation attributed to macromolecular crowding. *J. Mol. Biol.* 326:1227–1237.
19. Amsden, B. 2002. Modeling solute diffusion in aqueous polymer solutions. *Polym.* 43:1623–1630.
20. Gorenflo, R., F. Mainardi, D. Moretti, G. Pagnini, and P. Paradisi. 2002. Discrete random walk models for space-time fractional diffusion. *Chem. Phys.* 284:521–541.
21. Bouchaud, J., and A. Georges. 1990. Anomalous diffusion in disordered media: statistical mechanisms, models, and physical applications. *Phys. Rep.* 195:127–193.
22. Bunde, A., and S. Havlin. 1991. Percolation II. *In* Fractals and Disorderd Systems, 2nd Ed. Springer-Verlag, Berlin, Germany. 96–149.
23. Schaefer, D. W. 1984. A unified model for the structure of polymers in semidilute solution. *Polym.* 25:387–394.
24. Almeida, P., and W. Vaz. 1995. Lateral diffusion in membranes. *In* Handbook of Biological Physics. R. Lipowsky and E. Sackmann, editors. Elsevier, New York, NY. 305–357.
25. Saxton, M. 1994. Anomalous diffusion due to obstacles: a Monte Carlo study. *Biophys. J.* 66:394–401.

26. Kues, T., R. Peters, and U. Kubitscheck. 2001. Visualization and tracking of single protein molecules in the cell nucleus. *Biophys. J.* 80:2954–2967.
27. Weiss, M., M. Elsner, F. Kartberg, and T. Nilsson. 2004. Anomalous subdiffusion is a measure for cytoplasmic crowding in living cells. *Biophys. J.* 87:3518–3524.
28. Brown, E. B., E. S. Wu, W. Zipfel, and W. W. Webb. 1999. Measurement of molecular diffusion in solution by multiphoton fluorescence photobleaching recovery. *Biophys. J.* 77:2837–2849.
29. Wachsmuth, M., W. Waldeck, and J. Langowski. 2000. Anomalous diffusion of fluorescent probes inside living cell nuclei investigated by spatially-resolved fluorescence correlation spectroscopy. *J. Mol. Biol.* 298:677–689.
30. Feder, T. J., I. Brust-Mascher, J. P. Slattery, B. Baird, and W. W. Webb. 1996. Constrained diffusion or immobile fraction on cell surfaces: a new interpretation. *Biophys. J.* 70:2767–2773.
31. Jacobson, K., A. Ishihara, and R. Inman. 1987. Lateral diffusion of proteins in membranes. *Annu. Rev. Physiol.* 49:163–175.
32. Haupts, U., S. Maiti, P. Schwille, and W. W. Webb. 1998. Dynamics of fluorescence fluctuations in green fluorescent protein observed by fluorescence correlation spectroscopy. *Proc. Natl. Acad. Sci. USA.* 95:13573–13578.
33. Swaminathan, R., C. Hoang, and A. Verkman. 1997. Photobleaching recovery and anisotropy decay of green fluorescent protein GFP-S65T in solution and cells: cytoplasmic viscosity probed by green fluorescent protein translational and rotational diffusion. *Biophys. J.* 72:1900–1907.
34. Gennerich, A., and D. Schild. 2000. Fluorescence correlation spectroscopy in small cytosolic compartments depends critically on the diffusion model used. *Biophys. J.* 79:3294–3306.
35. Fradin, C., A. Abu-Arish, R. Granek, and M. Elbaum. 2003. Fluorescence correlation spectroscopy close to a fluctuating membrane. *Biophys. J.* 84:2005–2020.
36. Mastro, A. M., M. A. Babich, W. D. Taylor, and A. D. Keith. 1984. Diffusion of a small molecule in the cytoplasm of mammalian cells. *Proc. Natl. Acad. Sci. USA.* 81:3414–3418.
37. Luby-Phelps, K. 1994. Physical properties of the cytoplasm. *Curr. Opin. Cell Biol.* 6:3–9.
38. Luby-Phelps, K., D. Taylor, and F. Lanni. 1986. Probing the structure of the cytoplasm. *J. Cell Biol.* 102:2015–2022.
39. Lukacs, G., P. Haggie, O. Seksek, D. Lechardeur, N. Freedman, and A. Verkman. 2000. Size-dependent DNA mobility in cytoplasm and nucleus. *J. Biol. Chem.* 275:1625–1629.
40. Seksek, O., J. Biwersi, and A. Verkman. 1997. Translational diffusion of macromolecule-sized solutes in cytoplasm and nucleus. *J. Cell Biol.* 138:131–142.
41. Verkman, A. 2002. Solute and macromolecule diffusion in cellular aqueous compartments. *Trends Biochem. Sci.* 27:27–33.
42. Dayel, M., E. Hom, and A. Verkman. 1999. Diffusion of green fluorescent protein in the aqueous-phase lumen of endoplasmic reticulum. *Biophys. J.* 76:2843–2851.
43. Wojcieszyn, J. W., R. A. Schlegel, E. S. Wu, and K. A. Jacobson. 1981. Diffusion of injected macromolecules within the cytoplasm of living cells. *Proc. Natl. Acad. Sci. USA.* 78:4407–4410.
44. Elowitz, M., M. Surette, P. Wolf, J. Stock, and S. Leibler. 1999. Protein mobility in the cytoplasm of Escherichia coli. *J. Bacteriol.* 181:197–203.
45. Fundueanu, G., C. Nastruzzi, A. Carpov, J. Desbrieres, and M. Rinaudo. 1999. Physico-chemical characterization of Ca-alginate microparticles produced with different methods. *Biomaterials.* 20:1427–1435.
46. Brandrup, J., and E. H. Immergut. 1999. Polymer Handbook. Wiley, New York, NY.
47. Sivasankar, S., S. Subramaniam, and D. Leckband. 1998. Direct molecular level measurements of the electrostatic properties of a protein surface. *Proc. Natl. Acad. Sci. USA.* 95:12961–12966.
48. Goh, Y. Y., V. Frecer, B. Ho, and J. L. Ding. 2002. Rational design of green fluorescent protein mutants as biosensor for bacterial endotoxin. *Protein Eng.* 15:493–502.
49. Magde, D., E. Elson, and W. W. Webb. 1972. Thermodynamic fluctuations in a reacting system—measurement by fluorescence correlation spectroscopy. *Phys. Rev. Lett.* 29:705–708.
50. Thompson, N. L. 1991. Fluorescence correlation spectroscopy. *In* Topics in Fluorescence Spectroscopy. J. Lakowicz, editor. Plenum Press, New York, NY. 338–378.
51. Schwille, P. 2001. Fluorescence correlation spectroscopy and its potential for intracellular applications. *Cell Biochem. Biophys.* 34:383–408.
52. Webb, W. 2001. Fluorescence correlation spectroscopy: inception, biophysical experimentations, and prospectus. *Appl. Opt.* 40:3969–3983.
53. Periasamy, N., and A. S. Verkman. 1998. Analysis of fluorophore diffusion by continuous distributions of diffusion coefficients: application to photobleaching measurements of multicomponent and anomalous diffusion. *Biophys. J.* 75:557–567.
54. Schwille, P., J. Korlach, and W. W. Webb. 1999. Fluorescence correlation spectroscopy with single-molecule sensitivity on cell and model membranes. *Cytometry.* 36:176–182.
55. Widengren, J., U. Mets, and R. Rigler. 1995. Fluorescence correlation spectroscopy of triplet states in solution: a theoretical and experimental study. *J. Phys. Chem.* 99:13368–13379.
56. Metzler, R., and J. Klafter. 2000. The random walk's guide to anomalous diffusion: a fractional dynamics approach. *Phys. Rep.* 339:1–77.
57. Sengupta, P., K. Garai, J. Balaji, N. Periasamy, and S. Maiti. 2003. Measuring size distribution in highly heterogeneous systems with fluorescence correlation spectroscopy. *Biophys. J.* 84:1977–1984.
58. Módos, K., R. Galántai, I. Bárdos-Nagy, M. Wachsmuth, K. Tóth, J. Fidy, and J. Langowski. 2004. Maximum-entropy decomposition of fluorescence correlation spectroscopy data: application to liposome–human serum albumin association. *Eur. Biophys. J.* 33:59–67.
59. Skilling, J., and R. K. Bryan. 1984. Maximum entropy image reconstruction: general algorithm. *Mon. Not. R. Astron. Soc.* 211: 111–124.
60. Saffarian, S., and E. L. Elson. 2003. Statistical analysis of fluorescence correlation spectroscopy: the standard deviation and bias. *Biophys. J.* 84:2030–2042.
61. Sengupta, P., K. Garai, B. Sahoo, Y. Shi, D. J. E. Callaway, and S. Maiti. 2003. The amyloid peptide (A1–40) is thermodynamically soluble at physiological concentrations. *Biochemistry.* 42:10506–10513.
62. Nagle, J. 1992. Long tail kinetics in biophysics? *Biophys. J.* 63:366–370.
63. Phillips, R. J., and F. T. Kosar. 1995. Measurement of protein diffusion in dextran solutions by holographic interferometry. *AIChE J.* 41:701–711.
64. Petit, J.-M., X. X. Zhu, and P. M. Macdonald. 1996. Solute probe diffusion in aqueous solutions of poly(vinyl alcohol) as studied by pulsed-gradient spin-echo NMR spectroscopy. *Macromolecules.* 29: 70–76.
65. Phillies, G. D. J. 1987. Dynamics of polymers in concentrated solutions: the universal scaling equation derived. *Macromolecules.* 20:558–564.
66. Saxton, M. 1996. Anomalous diffusion due to binding: a Monte Carlo study. *Biophys. J.* 70:1250–1262.
67. Netz, P. A., and T. Dorfmuller. 1995. Computer-simulation studies of anomalous diffusion in gels: structural-properties and probe-size dependence. *J. Chem. Phys.* 103:9074–9082.
68. Fatin-Rouge, N., K. Starchev, and J. Buffle. 2004. Size effects on diffusion processes within agarose gels. *Biophys. J.* 86:2710–2719.

69. Amblard, F., A. C. Maggs, B. Yurke, A. N. Pargellis, and S. Leibler. 1996. Subdiffusion and anomalous local viscoelasticity in actin networks. *Phys. Rev. Lett.* 77:4470–4473.

70. Wong, I. Y., M. L. Gardel, D. R. Reichman, E. R. Weeks, M. T. Valentine, A. R. Bausch, and D. A. Weitz. 2004. Anomalous diffusion probes microstructure dynamics of entangled F-actin networks. *Phys. Rev. Lett.* 92:178101.

71. Basu, S., C. W. Wolgemuth, and P. J. Campagnola. 2004. Measurement of normal and anomalous diffusion of dyes within protein structures fabricated via multiphoton excited cross-linking. *Biomacromolecules.* 5:2347–2357.

72. Dwyer, J. D., and V. A. Bloomfield. 1993. Brownian dynamics simulations of probe and self-diffusion in concentrated protein and DNA solutions. *Biophys. J.* 65:1810–1816.

73. Chirico, G., M. Placidi, and S. Cannistraro. 1999. Fractional Stokes-Einstein relationship in biological colloids: role of mixed stick-slip boundary conditions. *J. Phys. Chem. B.* 103:1746–1751.

74. De Smedt, S. C., A. Lauwers, J. Demeester, Y. Engelborghs, G. D. Mey, and M. Du. 1994. Structural information on hyaluronic acid solutions as studied by probe diffusion experiments. *Macromolecules.* 27:141–146.

75. Dauty, E., and A. S. Verkman. 2004. Molecular crowding reduces to a similar extent the diffusion of small solutes and macromolecules: measurement by fluorescence correlation spectroscopy. *J. Mol. Recognit.* 17:441–447.

76. Furukawa, R., J. L. Arauz-Lara, and B. R. Ware. 1991. Self-diffusion and probe diffusion in dilute and semidilute aqueous solutions of dextran. *Macromolecules.* 24:599–605.

77. Busch, N. A., T. Kim, and V. A. Bloomfield. 2000. Tracer diffusion of proteins in DNA solutions. 2. Green fluorescent protein in crowded DNA solutions. *Macromolecules.* 33:5932–5937.

78. Masuda, A., K. Ushida, and T. Okamoto. 2005. New fluorescence correlation spectroscopy enabling direct observation of spatiotemporal dependence of diffusion constants as an evidence of anomalous transport in extracellular matrices. *Biophys. J.* 88:3584–3591.

79. Weeks, E. R., and D. A. Weitz. 2002. Properties of cage rearrangements observed near the colloidal glass transition. *Phys. Rev. Lett.* 89:095704.

80. Kegel, W. K., and A. van Blaaderen. 2000. Direct observation of dynamical heterogeneities in colloidal hard-sphere suspensions. *Science.* 287:290–293.

81. Weeks, E. R., and D. A. Weitz. 2002. Subdiffusion and the cage effect studied near the colloidal glass transition. *Chem. Phys.* 284: 361–367.

82. Rauch, J., and W. Kohler. 2002. Diffusion and thermal diffusion of semidilute to concentrated solutions of polystyrene in toluene in the vicinity of the glass transition. *Phys. Rev. Lett.* 88:185901–185904.

83. Caspi, A., R. Granek, and M. Elbaum. 2002. Diffusion and directed motion in cellular transport. *Phys. Rev. E Stat. Nonlin. Soft Matter Phys.* 66:011916.

84. Schaefer, D. 1984. A unified model for the structure of polymers in semidilute solution. *Polym.* 25:387–394.

85. Fulton, A. B. 1982. How crowded is the cytoplasm? *Cell.* 30: 345–347.

86. Zimmerman, S. B., and S. O. Trach. 1991. Estimation of macromolecule concentrations and excluded volume effects for the cytoplasm of Escherichia coli. *J. Mol. Biol.* 222:599–620.

87. Weiss, M. 2003. Stabilizing Turing patterns with subdiffusion in systems with low particle numbers. *Phys. Rev. E Stat. Nonlin. Soft Matter Phys.* 68:036213.

88. Shirtliff, M. E., J. T. Mader, and A. K. Camper. 2002. Molecular interactions in biofilms. *Chem. Biol.* 9:859–871.

89. Zaidel-Bar, R., M. Cohen, L. Addadi, and B. Geiger. 2004. Hierarchical assembly of cell-matrix adhesion complexes. *Biochem. Soc. Trans.* 32:416–420.